X-ray Diffraction Study of the Early Stages of the Growth of Nanoscale Zinc Oxide Crystallites Obtained from Thermal Decomposition of Four Precursors. General Concepts on Precursor-Dependent Microstructural Properties

Nathalie Audebrand, Jean-Paul Auffrédic, and Daniel Louër*

Laboratoire de Chimie du Solide et Inorganique Moléculaire (UMR 6511, CNRS), Groupe de Cristallochimie, Université de Rennes 1, Avenue du Général Leclerc, 35042 Rennes Cedex, France

Received March 5, 1998. Revised Manuscript Received June 23, 1998

A detailed analysis of the microstructural properties of nanocrystalline zinc oxide powders produced by thermal decomposition of four different precursors (hydroxide nitrate, oxalate, hydroxide carbonate, and acetate) is described. The analysis is based on the modern developments of X-ray powder diffraction line broadening analysis. The early stages of the crystallite growth up to 600 °C have been studied in situ at constant heating rate and ex situ from samples prepared under isothermal conditions. It is shown that the crystallites are prismatic and can be averaged by a cylindrical shape with diameter D and height H. The thermal behavior of crystallite size and shape aspects depends on the nature of the precursor. Above ∼350 °C, the constant value of D/H demonstrates that similar crystallite shapes are observed during crystallite growth. The kinetics of the crystallite growth has been studied for the four samples, from which activation energies have been calculated. Crystallite sizes are also compared to values from SEM and BET measurements. The agglomeration process of the crystallites is investigated from a comparison between surface areas calculated from the BET method and the powder diffraction analysis. From the complete results, general rules on the precursor dependence of the observed microstructural properties are established.

1. Introduction

There is a continuous interest in the chemistry and physical properties of nanoscale "particles" in technologically important applications.[1,3] Nanoscale particles also play a major role in the reactivity of solids, e.g., decomposition reactions and crystallization phenomena. Generally, various methods are used to characterize particle sizes, such as electron microscopy, BET surface area, and X-ray diffraction line broadening analysis. However, the definition of particle differs according to the method used. Among them, X-ray diffraction provides a unique characterization of particles in the sense of coherently diffracting domains or crystallites, in the approximate range 2−100 nanometers. Diffraction line broadening analysis has generally been restricted to the study of a limited number of *hkl* reflections, due to the line overlap problem. However, with the development of fitting techniques to model the whole powder diffraction pattern, more reflections can now be interpreted in microstructural terms.[4−8] A few examples, based on this new methodology, with remarkably detailed three-dimensional descriptions of the microstructural properties of nanocrystalline powders, such as crystallite size, shape, and stacking faults, have been reported. Representative examples include ZnO[9,10] or CeO_2[11] powders obtained from the thermal decomposition of precursors. These thorough characterizations give the opportunity to investigate, on a nanometric scale, some properties related to the microstructure of a powder material produced from different precursors. Thus, it may provide new insights into specific relationships between the microstructural properties of an oxide and the nature of its precursor.

The morphological properties of ZnO crystallites produced isothermally from the decomposition of two

* Corresponding author. Tel.: (33) 02 99 28 62 48. Fax: (33) 02 99 38 34 87. E-mail: Daniel.Louer@univ-rennes1.fr.

(1) Itoh, H.; Utamapanya, S.; Stark, J. V.; Klabunde, K. J.; Schlup, J. R. *Chem. Mater.* **1993**, *5*, 71−77.
(2) Ahmadi, T. S.; Wang, Z. L.; Henglein, A.; El-Sayed, M. A. *Chem. Mater.* **1996**, 8, 1161−1163.
(3) Masui, T.; Fujiwara, K.; Machida, K.; Adachi, G.; Sakata, T.; Mori, H. *Chem. Mater.* **1997**, *9*, 2197−2204.
(4) Langford, J. I.; Louër, D. *Rep. Prog. Phys.* **1996**, 59, 131−234.
(5) Langford, J. I.; Louër, D.; Sonneveld, E. J.; Visser, J. W. *Powder Diffr.* **1986**, 1, 211−221.
(6) Toraya, H. *J. Appl. Crystallogr.* **1986**, 19, 440−447.
(7) Langford, J. I. In *Accuracy in Powder Diffraction II*; Prince, E., Stalick, J. K., Eds.; Spec. Publ. 846; NIST: Gaithersburg, MD, pp 110−126, 1992.
(8) Louër D. *Adv. X-ray Anal.* **1994**, 37, 27−35.
(9) Louër, D.; Auffrédic, J. P.; Langford, J. I.; Ciosmak, D.; Niepce, J. C. *J. Appl. Crystallogr.* **1983**, 16, 183−191.
(10) Langford, J. I.; Boultif, A.; Auffrédic, J. P.; Louër, D. *J. Appl. Crystallogr.* **1993**, 26, 22−33.
(11) Guillou, N.; Auffrédic, J. P.; Louër, D. *Powder Diffr.* **1995**, 10, 236−240.

S0897-4756(98)00132-X CCC: $15.00
Published on Web 08/14/1998

precursors, a hydroxide nitrate, $Zn_3(OH)_4(NO_3)_2$, and an oxalate, $ZnC_2O_4 \cdot 2H_2O$, have been reported previously.[9,10] In both cases, crystallites were described with an average cylindrical shape, with different "aspect" ratio D/H, where D is the diameter and H the height of the cylinder. The study was also extended to samples obtained at different annealing temperatures,[12,13] from which the early stages of crystallite growth could be described. In addition, some interesting trends about relationships between oxide crystallite shape/dimension, growth process, and the nature of the precursor arose from these two studies. In particular, the microstructure of ZnO obtained by decomposition would have some "genetic" properties related to the precursor. The underlying concepts are obviously important, since features such as size and shape anisotropy of the crystallites, crystallite growth, and process of particle agglomeration of the oxide would be governed by the nature of the precursor. However, the results of the analysis of only two samples, prepared under isothermal conditions, were used to derive these suggestions. Clearly, additional studies are required to support the generalization. The purpose of the present study is to explore further these ideas. Two new ZnO samples, obtained from the thermal decomposition of a hydroxide carbonate, $Zn_5(OH)_6(CO_3)_2$, and an acetate, $Zn(CH_3COO)_2 \cdot 2H_2O$, have been investigated. The microstructural properties of these two materials have been carefully studied from diffraction line broadening analysis. The study has been extended to samples prepared isothermally at various temperatures and to samples subjected to a constant heating regime, from which the crystallite growth process has been interpreted. The results are compared with those already reported for the two ZnO samples obtained from $Zn_3(OH)_4(NO_3)_2$[9,12] and $ZnC_2O_4 \cdot 2H_2O$.[10,13] However, for these two last oxide samples, the results have been completed in the present work by in situ experiments carried out with a constant heating regime. The overall results are then used to tentatively establish some general concepts related to the role of the precursor on the microstructure of nanocrystalline ZnO powders.

2. Experimental Section

2.1. Diffraction Data Collection. Temperature-dependent X-ray diffraction (TDXD) was carried out with an INEL (CPS 120) curved position-sensitive detector, used in a diffraction geometry by reflection (Cu $K\alpha_1$, $\lambda = 1.5406$ Å) described elsewhere.[14] The stationary sample was heated in a monitored high-temperature device (Rigaku). Slow heating regimes were used and counting times for each pattern varied from 600 to 2300 s, depending on the sample investigated and the expected counting statistics. The instrumental g profiles were obtained from a sample of ZnO annealed at high temperature. The thermal dependence of the instrumental profile breadths was found to be negligible with regard to the precision of the collected data.

For samples prepared isothermally, precise diffraction data were collected at room temperature with a Siemens D500 high-resolution powder diffractometer, using monochromatic Cu $K\alpha_1$ X-rays obtained with a germanium incident-beam monochromator. The characteristics of this arrangement and its instrumental resolution function have been described elsewhere.[15] The diffraction patterns were scanned over the angular range 26°−148° (2θ). The step size and the counting times were chosen according to line broadening, which decreases as the annealing temperature increases. The step size was selected to be approximately $^1/_{10}$ of the fwhm values, i.e., in the range 0.015−0.03° (2θ) until 86° (2θ) and in the range 0.03−0.05° (2θ) to the end of the scan. The counting time was chosen between 30 and 80 s step^{-1} until 86° (2θ) and between 50 and 150 s step^{-1} to the end of the scan. The instrumental g profiles were obtained from the standard reference material LaB_6 (SRM 660)[16] used to model the instrumental function of the high-resolution diffractometer, according to a procedure described elsewhere.[17]

2.2. BET and SEM Measurements. The specific surface area (S_{BET}) of the ZnO powders was obtained by adsorbing nitrogen[18] at 77 K, by using the Flowsorb II 2300 equipment manufactured by Micromeritics S.A. Scanning electron microscopy (SEM) observations were carried out by means of a JEOL SEM 6400 instrument.

2.3. Materials Preparation. Zinc oxide powders were obtained from the thermal decomposition of four precursors: a hydroxide carbonate (hc), $Zn_5(OH)_6(CO_3)_2$ (Aldrich); an acetate (ac), $Zn(CH_3COO)_2 \cdot 2H_2O$ (Merck); a hydroxide nitrate (hn), $Zn_3(OH)_4(NO_3)_2$, prepared from a slow hydrolysis at 110 °C of an aqueous solution of zinc nitrate (Merck);[9] and an oxalate (ox), $ZnC_2O_4 \cdot 2H_2O$ (Johnson Matthey). In the following, the ZnO samples obtained from these four precursors are denoted as hc-ZnO, ac-ZnO, hn-ZnO, and ox-ZnO, respectively. Two preparation modes were used in the present study.

(A) Preparation at Constant Heating Rate. The three-dimensional plots of the successive X-ray diffraction patterns recorded upon heating, during the decomposition of the precursors $Zn_3(OH)_4(NO_3)_2$ (hn), $ZnC_2O_4 \cdot 2H_2O$ (ox), $Zn_5(OH)_6(CO_3)_2$ (hc), and $Zn(CH_3COO)_2 \cdot 2H_2O$ (ac), and the subsequent crystallite growth of zinc oxide are displayed in Figure 1. According to previous studies[9,10,12,13] the thermal decomposition of the two first precursors was carried out under vacuum and nitrogen, respectively. Under these conditions, hn-ZnO appears above 160 °C (Figure 1a) and ox-ZnO at about 345 °C (Figure 1b). The decomposition of the hydroxide carbonate was performed under vacuum. Zinc oxide is formed in one stage above ∼230 °C (Figure 1c). The decomposition of $Zn(CH_3COO)_2 \cdot 2H_2O$ has been investigated previously by Djéga-Mariadassou et al.[19] It was found that the intermediate phases formed in the first stages sublimate partially when the decomposition is carried out under nitrogen or vacuum. Also, when a high heating rate (∼100 °C h^{-1}) is employed, the melting of anhydrous acetate occurs, so the formation of zinc oxide takes place from a liquid. Consequently, the morphological and textural properties of ZnO were found to be dependent upon the experimental conditions used. For all these reasons and also to prevent the formation of carbon from the decomposition of the acetate group, the thermal decomposition of this precursor was carried out in flowing air with a slow heating rate (6 °C h^{-1}). Under these conditions, the precursor dehydrates first into the anhydrous α-$Zn(CH_3COO)_2$, which in turn decomposes to zinc oxide in the range 110−130 °C (Figure 1d). For the four ZnO samples, the growth of the crystallites was studied up to ∼600 °C.

(B) Preparation under Isothermal Conditions. The temperature range for which a precise determination of the microstructural properties of ZnO samples can be performed from

(12) Louër, D.; Vargas, R.; Auffrédic, J. P. *J. Am. Ceram. Soc.* **1984**, 67, 136−141.
(13) Auffrédic, J. P.; Boultif, A.; Langford, J. I.; Louër, D. *J. Am. Ceram. Soc.* **1995**, 78, 323−328.
(14) Plévert, J.; Auffrédic, J. P.; Louër, M.; Louër, D. *J. Mater. Sci.* **1989**, 24, 1913−1918.
(15) Louër, D.; Langford, J. I. *J. Appl. Crystallogr.* **1988**, 21, 430−437.
(16) Fawcett, T. G.; Crowder, C. E.; Brownell, S. J.; Zhang, Y.; Hubbard, C.; Schreiner, W.; Hamill, G. P.; Huang, T. C.; Langford, J. I.; Hamilton, R.; Louër, D. *Powder Diff.* **1988**, 3, 209−218.
(17) Louër, D.; Audebrand, N. *Adv. X-ray Anal.* **1998**, 41, in press.
(18) Brunauer, S.; Emmet, P. H.; Teller, E. *J. Am. Chem. Soc.* **1938**, 60, 309−319.
(19) Djéga-Mariadassou, G.; Pannetier, G.; Giovanoli, R. *J. Microsc.* **1972**, 15, 323−336.

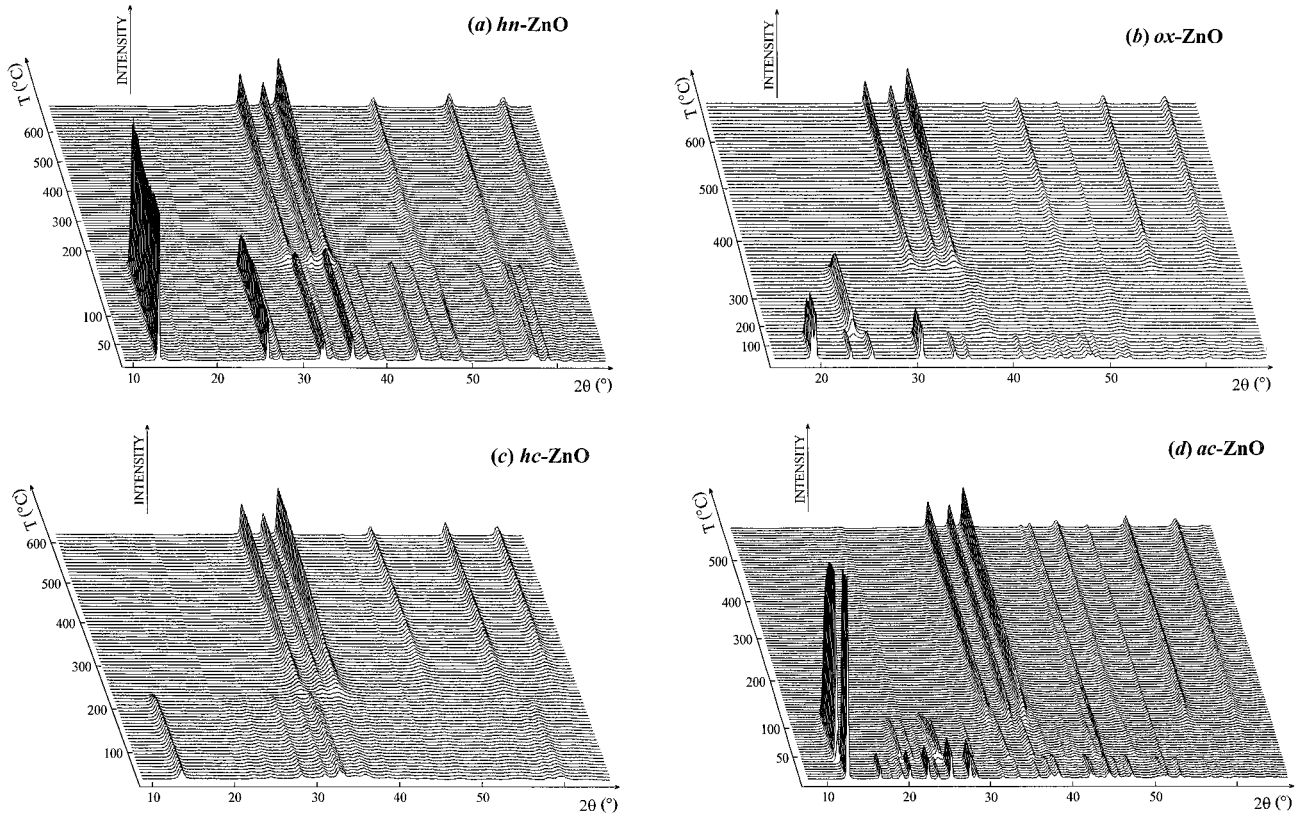

Figure 1. TDXD plots for (a) hn-ZnO, under vacuum (heating regime, 25−150 °C/10 °C h^{-1}, 150−675 °C/25 °C h^{-1}; counting time, 1200s per pattern); (b) ox-ZnO, under nitrogen (22−70 °C/100 °C h^{-1}, 70−110 °C/25 °C h^{-1}, 110−250 °C/100 °C h^{-1}, 250−670 °C/25 °C h^{-1}; 1000s per pattern); (c) hc-ZnO, under vacuum (25−615 °C/25 °C h^{-1}; 1100s per pattern); (d) ac-ZnO, under air (15−130 °C/6 °C h^{-1}, 130−570 °C/9 °C h^{-1}; 2300s per pattern).

X-ray line broadening analysis is limited. This is due to serious overlap of broad diffraction lines occurring for samples prepared at low temperatures and, for high temperatures, due to the instability of the deconvolution procedure in line broadening analysis when intrinsic broadening is small compared to instrumental broadening. Consequently, hc-ZnO and ac-ZnO samples were prepared in the temperature ranges 460−725 °C and 400−675 °C, respectively. Samples of hc-ZnO were obtained under the following conditions: 300 mg of precursor, under vacuum, 360 °C h^{-1} from room temperature to 100 °C, 5 °C h^{-1} from 100° to 230 °C and 360 °C h^{-1} from 230 °C to the selected annealing temperature. In a preliminary study, from the analysis of the fwhm of the diffraction lines of a sample obtained at 460 °C, it was found that the annealing process was complete after ∼6 h. Thus, the same time was selected for the other samples obtained at higher temperatures. For ac-ZnO the precursor (300 mg) was heated in a stream of air, with a heating rate of 5 °C h^{-1} from room temperature to 230 °C and 100 °C h^{-1} until the selected annealing temperature. A complete annealing at a given temperature required times ranging from 10 h (higher temperatures) to a few days (lower temperatures).

2.4. Diffraction Line Broadening Analysis. To investigate the microstructure of a sample, reliable parameters defining the position, the breadths, fwhm, and integral breadth β (=integral intensity/peak height), shape, and profile of the diffraction lines are required. These quantities are easily extracted with pattern-modeling software, provided the counting statistics of the data are good enough and that line overlap is not too severe.[8] In this procedure Bragg reflections are represented by analytical functions, which are fitted to the observed data by the method of least squares. The functions used in this study are the Pearson VII, the pseudo-Voigt, and the Voigt functions, characterized by their shape factor, i.e., the exponent m, the mixing factor η, and ϕ (=fwhm/β), respectively. Additional details can be found elsewhere.[4] In the present study, pattern decomposition was carried out by means of the Socabim program PROFILE, which is a part of the DIFFRAC-AT package supplied by Siemens. For the physical interpretation of line broadening, two approaches, Fourier analysis and the integral breadth method, have been used. The interpretation is based on the sample-dependent f profile, derived from the observed h profile after deconvolution by the instrumental g profile ($h = f*g$). The two methods have been applied to the profile parameters extracted from PROFILE.

(A) Fourier Analysis. According to the Warren−Averbach−Bertaut[20] procedure, the Stokes' corrected cosine Fourier coefficients $A(n,l)$, where n is the Fourier harmonic number and l the order of reflection, of the sample-dependent line profile can be expressed as the product of order-independent size coefficients $A^S(n)$ and order-dependent distortion coefficients $A^D(n,l)$. Considering a series expansion of $A(n,l)$, valid for low values of l and n, $A^S(n)$ and the microstrain $\langle e^2(n)\rangle$ can be separated, if at least two orders of a reflection are available, by means of the equation:[21]

$$A(n,l) = A^S(n) - A^S(n)2\pi^2 l^2 n^2 \langle e^2(n)\rangle \qquad (1)$$

The Fourier coefficients are expressed as a function of a distance, perpendicular to the diffracting planes, $L = n/\Delta s$, where Δs [$=2(\sin\theta_2 - \sin\theta_1)/\lambda$, θ_1 and θ_2 are the limits of the angular range and λ is the wavelength of the radiation] is the range, in reciprocal units, which contains all intensity points of the reflection. The initial slope of $A^S(n)$ versus L is generally a measure of the Fourier apparent size, ϵ_F, which is related to the true size of the crystallite. Nevertheless, if stacking faults also contribute to line broadening, as for instance in ox-ZnO,[10] ϵ_F is thus an effective crystallite size, which includes the

(20) Warren, B. E. 1969. X-ray Diffraction, Reading MA: Addison-Wesley.

(21) Delhez, R.; Mittemeijer, E. J. *J. Appl. Crystallogr.* **1976**, 9, 233−234.

apparent size of the diffracting domains and a fictitious size due to faults on certain *hkl* planes. Another important result is that the integral breadth β^*, in reciprocal units, is directly related to the complex Fourier coefficients $C(n)$ [$\beta^* = \Delta s/\sum_n|C(n)|$]. Similarly to the Fourier apparent size ϵ_F, the integral breadth is related to the apparent size ϵ_β [$=(\beta^*)^{-1}$, if only a size effect contributes to the line broadening]. With the Fourier approach there is no assumption about the line shape. The technique has been recently combined with profile fitting, through a new program, *Prof*FOU,[17] used here for the study of ac-ZnO. In this procedure line-shape parameters (2θ, fwhm, m for the Pearson VII, η for the pseudo-Voigt) are extracted with PROFILE for both the observed h and instrumental g profiles. Then, they are employed to generate analytically the h and g profiles used in the Stokes−Fourier deconvolution operation in order to obtain the Fourier coefficients of the f profile due to structure imperfections.

(B) Integral-Breadth Methods. There are methods based on the use of the integral breadths extracted from pattern fitting. In the Langford method[7] a Voigt function is assumed to model adequately the observed h and g profiles, which means that the profiles are symmetrical and that the line-shape parameters ϕ lie within the Lorentzian limit ($\phi = 0.6366$) and the Gaussian limit ($\phi = 0.9394$). It should be noted that this simple method cannot be applied if data are markedly asymmetric or the line shape is out of the Lorentzian (or Gaussian) limit. In fact, these situations are not rare with highly divided solids; e.g., super-Lorentzian line shapes are often observed. (To overcome these problems, the Fourier method (A) is then an alternative approach.) However, when the Langford method was applicable, observed β_h were corrected for the instrumental contribution to give the integral breadth of the f profiles β_f in angular units ($^\circ 2\theta$), and then converted to reciprocal units β_f^* ($=\cos\theta\,\beta_f/\lambda$). If line broadening is solely attributed to a size effect, an apparent size ϵ_β ($=(\beta_f^*)^{-1}$) is obtained. If distortions also contribute to line broadening, some approximations are required to separate the different effects.[7] For further discussion, the reader is referred to the work of Louër.[22] The Langford method was used for the study of the microstructure of hc-ZnO.

Moreover, in the TDXD study, data quality was considerably poorer and the correction for the instrumental contribution was carried out from the empirical correction function:[23]

$$\beta_h^2 \sim \beta_f\beta_h + \beta_g^2 \qquad (2)$$

It must be noted that the apparent sizes derived from the Fourier and integral breadth methods do not have the same definition.[24] Indeed, ϵ_F is a surface-weighted mean, interpreted as the total area of projection of unit volume of the average crystallite on to the reflecting plane, while ϵ_β is the volume-weighted thickness of the crystallite measured in a direction perpendicular to the diffracting planes. Nevertheless, the two apparent measures can be related to the true size if the crystallite shape is known or assumed. For instance, for a spherical crystallite, the true diameter D is simply derived from $3\epsilon_F/2$ and $4\epsilon_\beta/3$. These simple relations are strictly valid for a monodisperse system. The presence of a size distribution can introduce some discrepancies between D_F and D_β. For powders prepared by controlled soft thermal decomposition, narrow size distributions can reasonably be expected. A representative illustration was reported recently for ex-oxide nitrate CeO_2.[11] For a cylindrical crystallite (more appropriate for hexagonal ZnO crystallites) of diameter D and height H, the apparent sizes ϵ_F and ϵ_β are related to D and H, and to the angle ϕ_z between the normal to the planes *hkl* and the cylinder axis by equations given by Langford and Louër[25] [i.e., eqs 10, 17, and 18 for ϵ_β and eqs 10 and 20 for ϵ_F] (see also ref 7). The best estimates of D and H are then obtained by a least-squares fit of these equations using the apparent sizes available for different directions of the diffraction vectors (see ref 10). This kind of analysis is greatly simplified if lattice distortion is negligible. An additional useful crystallite shape factor considered in the present study is the aspect ratio (D/H) of the cylindrical model.

3. Results

3.1. Crystallite Size and Shape of ZnO. ZnO samples prepared isothermally were used for characterizing the average size and shape of the crystallites. In the two previously reported studies, Fourier analysis was used for hn-ZnO[9] and the Langford method for ox-ZnO.[10] The analyses revealed that the two oxides were strain-free. A detailed description of the crystallite shape was reported, showing that the crystallites have a cylindrical shape[9,10] with mean parameters (D, H) at 280 °C (120 Å, 201 Å)[12] and 328 °C (195 Å, 167 Å)[13] for hn-ZnO and ox-ZnO, respectively. A similar analysis has been applied here to hc-ZnO and ac-ZnO. The integral breadth method has been applied to the diffraction data of hc-ZnO prepared isothermally at 460 °C, while the Fourier approach has been used to study ac-ZnO prepared isothermally at 575 °C. The first step in the analysis of line breadths in terms of structural imperfections is to examine an indexed Williamson−Hall plot,[26] giving the variation of β_f^* as a function of d^* ($=2\sin\theta/\lambda$). This plot displays an overview of the nature of the broadening due to sample imperfections. Williamson−Hall plots were previously reported for hn-ZnO (Figure 4 in ref 9) and ox-ZnO (Figure 4 in ref 10). The plots for hc-ZnO and ac-ZnO are given in Figure 2 (plots for samples prepared at other temperatures are of similar form). These plots can be commented on as follows.

(A) Ex-Hydroxide Carbonate ZnO (hc-ZnO). It is interesting to note that the behavior of the Williamson−Hall plot shown in Figure 2a, is similar to that observed for ox-ZnO (see Figure 4 in ref 10), for which it was shown that the sample was strain-free and that stacking faults contributed to line broadening. According to this interpretation, the values of β_f^* lie within one of three groups, depending on the *hkl* conditions. While reflections of two groups are affected by stacking faults, reflections of group 1 (*hk*0 or *hkl* with l even and $h - k = 3n$) are not. Since only size parameters are of interest in the present study, stacking faults are not discussed further. (The results of probability mistakes from groups 2 and 3 were reported elsewhere.[27]) For group 1 reflections, Figure 2a shows that there is little scatter of the β_f^* values for group 1 reflections around a zero-slope line, which indicates that the effect of microdistortion is negligible. This group of reflections can then be used to determine the average cylindrical crystallite shape. The least-squares procedure described in section 2.4 was applied to the 12 reflections of group 1, from which the section through the "fitted" cylinder is shown in Figure 3. A satisfactory agreement is obtained

(22) Louër, D. In *Microstructure Analysis by Diffraction*; Bunge, H., Fiala, J., Snyder, R. L., Eds.; IUCr Series; Oxford: Oxford University Press: Oxford, in press.
(23) Halder, N. C.; Wagner, C. N. J. *Adv. X-ray Anal.* **1966**, 9, 91−102.
(24) Guinier, A. *X-ray diffraction*; Freeman: San Francisco, 1963.
(25) Langford, J. I.; Louër, D. *J. Appl. Crystallogr.* **1982**, 15, 20−26.
(26) Williamson, G. K.; Hall, W. H. *Acta Met.* **1953**, 1, 22−31.
(27) Magnenet, C. *DEA Université Rennes I* **1995**.

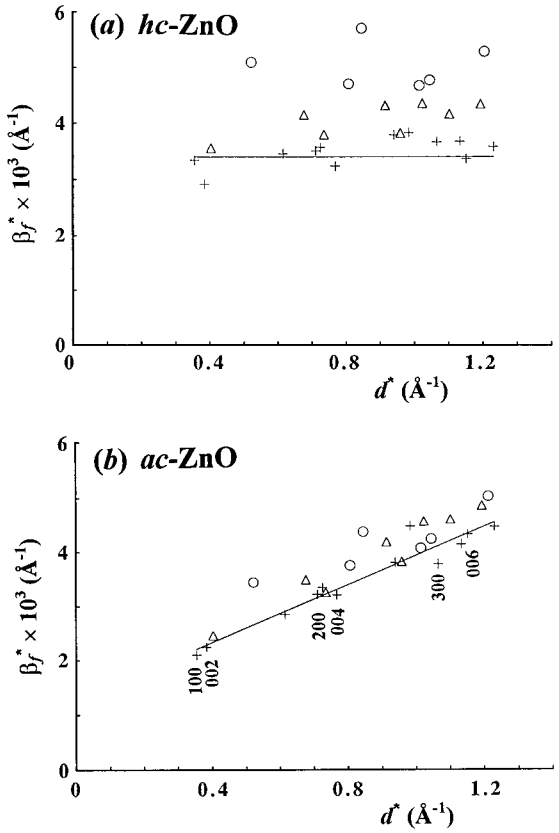

Figure 2. Williamson−Hall plots (β_f^* versus d^*) for (a) hc-ZnO at 460 °C and (b) ac-ZnO at 575 °C. (+) Group 1 reflections ($hk0$ or hkl with l even and h-k = 3n), (△) group 2 ($h - k = 3n \pm 1$, l odd), (○) group 3 ($h - k = 3n \pm 1$, l even).

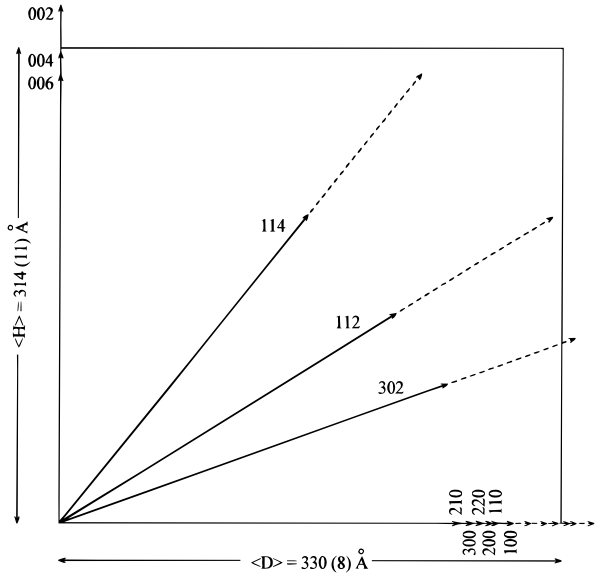

Figure 3. Section through the average cylinder used to model the form of the crystallites of hc-ZnO at 460 °C, from group 1 reflections. Observed apparent sizes (−) and actual observed size (- - -) in the direction hkl.

between the true observed sizes (derived from the observed apparent sizes[10]) represented by the largest lengths of the arrows in the direction of the diffracting vectors hkl and the calculated sizes represented by the section of the cylinder model. The average sizes are $\langle D \rangle$ = 330(8) Å and $\langle H \rangle$ = 314(11) Å.

(B) Ex-Acetate ZnO (ac-ZnO). The Williamson−Hall plot (Figure 2b) shows that stacking faults are also present in the sample. β_f^* for group 1 reflections lie on a nonzero-slope line, which means that the material contains microdistortions. Furthermore, many lines were found to have a super-Lorentzian shape, as shown by the mixing factor ranging from 0.54 to 1.41. For these reasons, the Fourier procedure was used to separate size and microdistortion effects. The study was limited by the small number of reflections with different orders available in group 1 reflections. Nevertheless, an analysis based on 100/200/300 and 002/004/006 reflections was carried out, which is enough to get information in the two principal directions of the cylindrical crystallite shape. The Fourier method was applied by means of the program *Prof*FOU.[17] Figure 4 shows the four cosine Fourier transforms of 100/200 and 002/004 reflections. The apparent sizes were derived from the initial slope of the size Fourier coefficients $A^S(n)$ versus L, obtained after application of eq 1. Finally, a cylindrical crystallite shape model is proposed for ac-ZnO. The average sizes are $\langle D \rangle$ = 453 Å and $\langle H \rangle$ = 338 Å.

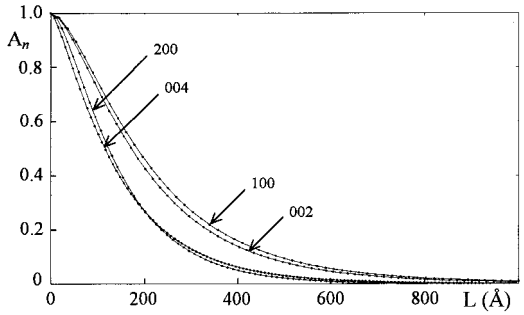

Figure 4. Fourier cosine coefficients A_n versus L for 100, 200, 002, and 004 reflections of ac-ZnO at 575 °C.

3.2. In Situ Crystallite Growth at Constant Heating Rate for the Four ZnO Samples. The quality of the diffraction data obtained from TDXD and the limited angular range in which they are collected (20°−70° 2θ) does not permit a precise line broadening analysis. The situation is aggravated by extremely broad diffraction lines, with low intensity, at the beginning of the crystallite growth. Consequently, an approximate approach was applied to only the first two intense lines, i.e., 100 and 002. The procedure is valid as long as the material contains negligible microstrains. If microstrains are present in the material, line broadening is thus order dependent (see eq 1), which means that the first order is less affected by this effect than the higher orders. In the case of ac-ZnO, the error introduced by neglecting microstrains was evaluated from the precise Fourier analysis carried out for the isothermal case. From the comparison of the results derived from the slopes at the origin of the $A^S(n)$ and $A(n)$ coefficients versus L plots, the error on apparent sizes was estimated to be ∼5% for the two lines 100 and 002. Consequently, after profile fitting of these two lines, repeated automatically to all successive ZnO patterns, and correction for the instrumental contribution (eq 2), the calculated integral breadths, β_f, were used to extract the apparent sizes of the crystallites in the directions perpendicular to (100) and (002). Taking into account the cylindrical shape of the crystallites, known from the precise study described above in section

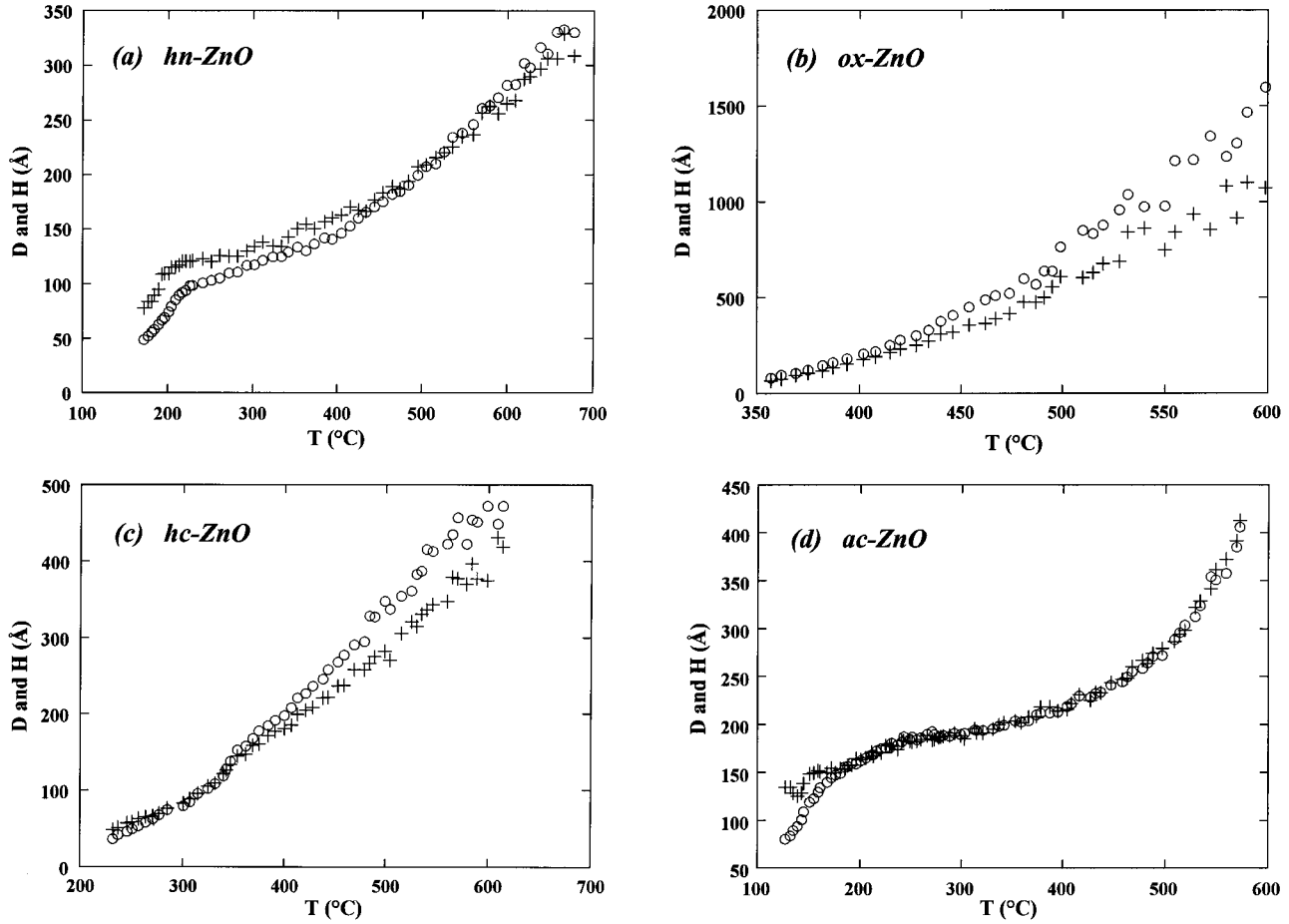

Figure 5. Crystallite diameter D (○) and height H (+) as a function of temperature, observed in situ with a constant heating rate: (a) hn-ZnO, (b) ox-ZnO, (c) hc-ZnO, (d) ac-ZnO.

3.1, the diameters D and heights H were calculated. It should be noted that the present approach, based on a quantitative three-dimensional description of the crystallite shape as a function of temperature, contrasts with the kinetic interpretation usually based on the changes with temperature of integrated intensities.

(A) Early Stages of Crystallite Growth. The changes of the diameter D and height H of the crystallites versus temperature for hn-, ox-, hc-, and ac-ZnO are displayed in Figure 5, respectively. The scatter of D and H for ox-ZnO observed at high temperatures is due to the instability of the deconvolution procedure when line broadening is close to the instrumental profile. Interesting features worthy of comment follow.

(i) Above 350 °C (the lower temperature at which ox-ZnO is obtained), the growth rate of D and H increases. Moreover, it can be seen from the diameters D observed at 350 °C (i.e., 135, 80, 140, and 200 Å for hn-, ox-, hc-, and ac-ZnO, respectively) and at 600 °C (i.e., 275, 1600, 480, and 400 Å, respectively) that the crystallite growth depends on the precursor. A similar behavior is observed for the heights H.

(ii) For hn-ZnO and ac-ZnO, both obtained at the lowest temperatures (170 and 130 °C), the changes of D and H describe an S-shaped behavior (Figure 5a,d). This phenomenon is not observed for ox-ZnO and hc-ZnO (Figure 5b,c), both obtained at higher temperatures (350 and 230 °C). This is surprising because initial crystallite sizes with similar magnitude are observed for the four ZnO samples (sizes $< \sim$100 Å). This feature would indicate that the crystallite growth process is dependent on the temperature range.

(iii) The degree of crystallite shape anisotropy depends not only on the precursor but also on the temperature range. This is illustrated in Figure 6, which displays the changes of the aspect ratio D/H. Except for ox-ZnO, the aspect ratio increases with temperature up to ~250 °C. At higher temperature, it reaches a quasiconstant value, which depends on the precursor, i.e., 1.0, 1.2, 1.2, and 1.0 for hn-, ox-, hc-, and ac-ZnO, respectively. This implies that the change with temperature of the aspect ratio is precursor-dependent only below 250 °C.

(B) Crystallite Growth Kinetics. Particle/crystallite growth kinetics generally follow the empirical equation:[28]

$$s^n - s_0^n = kt \tag{3}$$

where s is the mean particle size at the time t, s_0 is the mean initial particle size, n is the kinetic particle growth exponent, and k is a temperature-dependent constant. [For a thermally activated process, $k = A \exp(E_a/RT)$, where A is a constant, R is the gas constant, T is the absolute temperature, and E_a is the apparent activation energy for the growth process.] Under dynamic temperature conditions with a heating rate B, according to the

(28) Doremus, R. H. *Rates of phase transformations*; Harcourt Brace Jovanovich: Orlando, 1985.

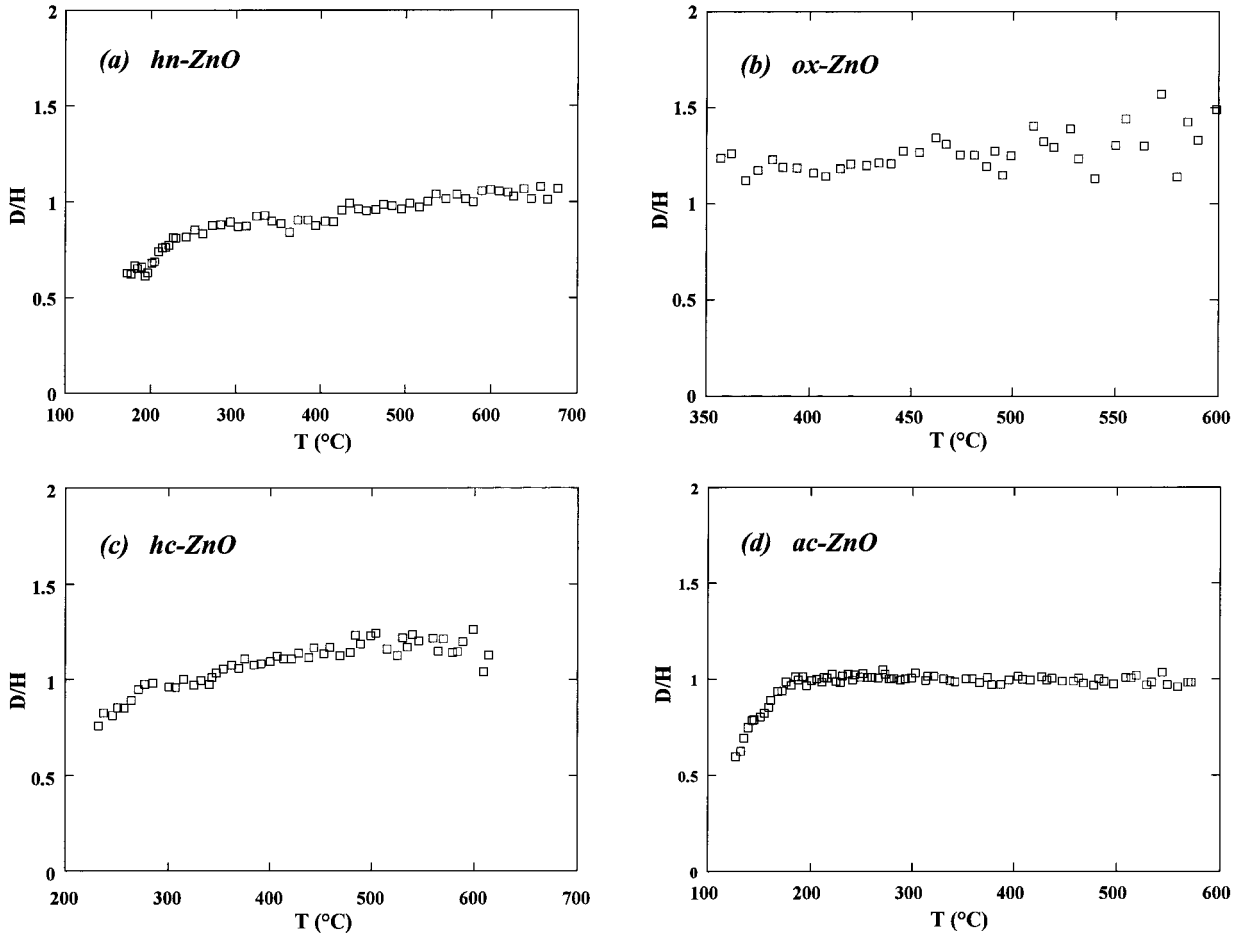

Figure 6. Crystallite aspect ratio D/H as a function of temperature, observed in situ with a constant heating rate: (a) hn-ZnO, (b) ox-ZnO, (c) hc-ZnO, (d) ac-ZnO.

classical derivations used for nonisothermal kinetics (see, for example, ref 29), the following equation is obtained:

$$\ln s = (1/n)[\ln(AE_a/RB) - 5.33 - 1.05E_a/RT] \quad (4)$$

Therefore when n is constant, a plot of ln s versus $1/T$ gives a linear relationship from which E_a can be calculated. Figure 7 displays the plots of ln D and ln H as a function of $1/T$ for the four ZnO samples. As predicted from eq 4, a linear behavior is found for ox-ZnO (Figure 7b) and hc-ZnO (Figure 7c). This is not observed for hn-ZnO (Figure 7a) and ac-ZnO (Figure 7d). This peculiarity has been confirmed by additional experiments. Although there is no apparent physical basis to interpret this feature, three linear regimes can be empirically distinguished over the whole temperature range (except in the plot ln H vs $1/T$ for ac-ZnO, for which only two slopes are statistically observed). For these two last samples, the highest slopes are obtained below ~250 °C, which corresponds to the highest crystallite growth rate (see Figure 5). The other straight lines lie between 250 and 400 °C and above 400 °C, respectively. This would indicate that different crystallite growth processes occur in the investigated temperature range. Table 1 gives the E_a/nR values for the four samples. In the next section [3.3 (B)], it will be shown that the activation energies found for the higher temperatures are comparable with those obtained independently in the isothermal study.

3.3. Isothermal Crystallite Growth of hc- and ac-ZnO. *(A) Early Stages of Crystallite Growth*. Samples obtained at selected temperatures were studied by the methodology used in section 2.4. Table 2 gives the values of crystallite size parameters $\langle D \rangle$ and $\langle H \rangle$. The corresponding aspect ratios $\langle D \rangle / \langle H \rangle$ and, for comparison, those related to hn-ZnO[12] and ox-ZnO[13] are reported in Table 3. It can be noted that for each sample the aspect ratios are almost constant in the temperature range considered. The average ratio is significantly smaller (~0.73) for hn-ZnO with regard to those obtained for the three other ZnO samples ($1.15 < \langle D \rangle / \langle H \rangle < 1.26$). Thus, the crystallites are anisotropic with H greater than D for hn-ZnO, while D is greater than H for the other samples. These aspect ratios are in broad agreement with those obtained in the approximate analysis carried out at constant heating rate in the same temperature ranges, i.e., 1.0, 1.2, 1.2, and 1.0 for hn-, ox-, hc-, and ac-ZnO, respectively (see Figure 6). Moreover, it must be noted that for ac-ZnO the magnitude of the root-mean-square microstrains ($\langle e^2 \rangle^{1/2}$) derived from eq 1 by *Prof*FOU decreases with the annealing temperature, though they do not disappear totally at higher temperatures (Figure 8).

(B) Crystallite Growth Kinetics. For $s \gg s_0$ and a constant crystallite growth time t, which here is the time required for a complete crystallite growth at a given

(29) Tanaka, H. *Thermochim. Acta* **1995**, 267, 29−44.

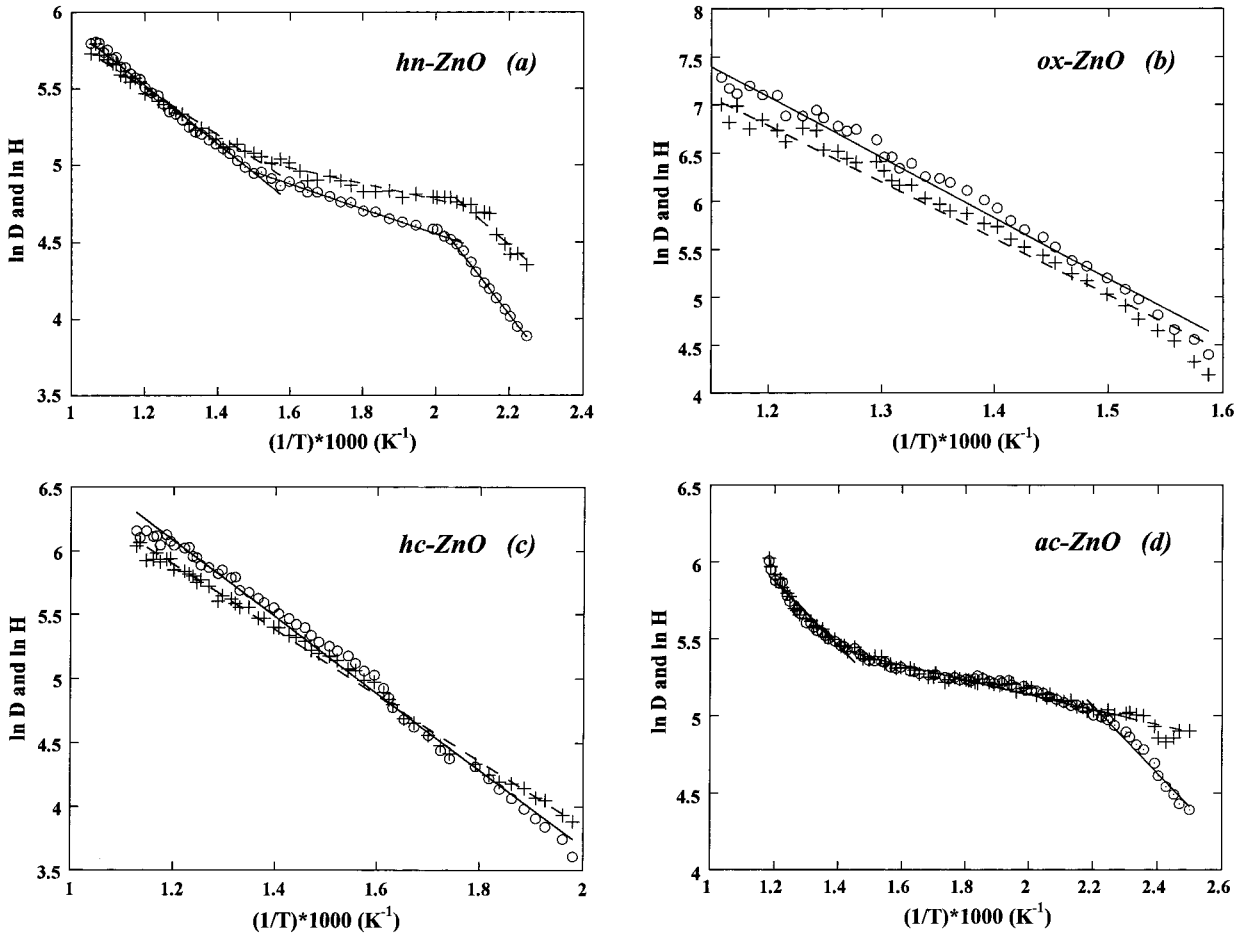

Figure 7. Plots ln D (○) and ln H (+) versus $1/T$, obtained in situ with a constant heating rate (a) hn-ZnO, (b) ox-ZnO, (c) hc-ZnO, (d) ac-ZnO.

Table 1. Kinetic Parameters for Constant Heating Rate and Isothermal Crystallite Growth

		diameter			height		
sample	range $10^3/T$ (K^{-1})	E_a/nR $K \times 10^3$	n	E_a (J mol^{-1}) $\times 10^3$	E_a/nR $K \times 10^3$	n	E_a (J mol^{-1}) $\times 10^3$
			Constant Heating Rate				
hn-ZnO	1.05−1.5	1.82		103	1.47		117
	1.5−2.0	0.77	6.8	44	0.50	9.6	40
	2.0−2.25	2.95		167	1.99		159
ox-ZnO	1.1−1.6	6.01	3.0	150	5.60	2.9	135
hc-ZnO	1.1−2.0	2.86	2.5	59	2.44	1.9	39
ac-ZnO	1.2−1.45	2.0		55	2.05		70
	1.45−2.2	0.46	3.3	13	0.46	4.1	16
	2.2−2.5	2.08		57	0.46		16
			Isothermal				
hn-ZnO	1.15−1.45	2.14	6.8	121	1.78	9.6	142
ox-ZnO	1.05−1.65	3.94	3.0	98	3.73	2.9	90
hc-ZnO	1.00−1.30	2.94	2.5	61	2.59	1.9	41
ac-ZnO	1.05−1.50	2.71	3.3	74	2.47	4.1	84

temperature, the slope of the plot of ln s against $1/T$ is equal to $-E_a/nR$ (from eq 3). Furthermore, the value of n can be obtained from the plot ln s versus ln t (s = D or H) for a given temperature T. This was calculated for hn-, ox-, hc-, and ac- ZnO at 500, 550, 400, and 655 °C, respectively, from results obtained in situ by TDXD. Similar experimental conditions as described in section 2.3 (A) were used to obtain a complete formation of ZnO at the lowest temperature. Then, a fast heating rate (∼1000 °C h^{-1}) was applied to reach the selected temperature. The time for collecting data was adapted to the speed of the crystallite growth (minimun counting time, 600 s). The crystallite sizes (D and H) were extracted from the analysis of the 100 and 002 lines as described above [see section 2.4 (ii), eq 2]. For each sample, the plots of ln D and ln H versus ln t were satisfactorily fit by straight lines. The values of n calculated from the slopes are given in Table 1. For ox-ZnO, the crystallite growth exponents (3.0 for D and 2.9 for H) correspond to the average value (3.0) reported previously for ZnO grain growth (see for example ref 30). For hc- and ac-ZnO, the crystallite diameter growth exponents are close to this value, but this is not true for the crystallite height growth exponent. This means

(30) Senda, T.; Bradt, R. *J. Am. Ceram. Soc.* **1990**, 73, 106−114.

Table 2. Calculated Crystallite Sizes, Calculated (S_{RXD}) and Experimental (S_{BET}) Surface Areas, and Experimental (D_{BET} and D_{SEM}) Sizes for hc- and ac-ZnO Samples

hc-ZnO							ac-ZnO						
T (°C)	$\langle D\rangle$ (Å)	$\langle H\rangle$ (Å)	S_{XRD} ($m^2\ g^{-1}$)	S_{BET} ($m^2\ g^{-1}$)	D_{BET} (Å)	D_{SEM} (Å)	T (°C)	$\langle D\rangle$ (Å)	$\langle H\rangle$ (Å)	S_{XRD} ($m^2\ g^{-1}$)	S_{BET} ($m^2\ g^{-1}$)	D_{BET} (Å)	D_{SEM} (Å)
460	330(8)	314(11)	32.59	18.23	580	517	400	220	199	49.77	5.88	1799	1206
510	435(16)	395(19)	25.13	12.69	833	718	450	269	218	42.38	7.71	1372	1294
560	586(22)	510(25)	18.94	8.03	1317	914	500	300	238	38.32	5.43	1978	1314
616	712(64)	597(73)	15.81	5.40	1959	1009	525	368	305	30.72	3.33	3176	1427
666	838(41)	674(50)	13.65	4.05	2611	1264	550	439	340	26.43	4.51	2345	1442
725	940(72)	801(89)	11.90	2.94	3597	1700	575	453	338	26.00	2.67	3961	1527
							600	546	394	21.86	3.12	3390	1603
							625	578	411	20.78	3.04	3479	1973
							650	619	530	18.04	2.94	3597	2265
							675	650	550	17.26	2.36	4482	3066

Table 3. Aspect Ratios $\langle D\rangle/\langle H\rangle$ of Four Samples of ZnO During the Annealing Process

hn-ZnO[12]		ox-ZnO[13]		hc-ZnO		ac-ZnO	
T (°C)	$\langle D\rangle/\langle H\rangle$	T (°C)	$\langle D\rangle/\langle H\rangle$	T (°C)	$\langle D\rangle/\langle H\rangle$	T (°C)	$\langle D\rangle/\langle H\rangle$
280	0.60	328	1.17	460	1.05	400	1.11
410	0.76	350	1.17	510	1.10	450	1.23
430	0.72	375	1.14	560	1.15	500	1.26
460	0.69	400	1.20	616	1.19	525	1.21
510	0.70	410	1.22	666	1.24	550	1.29
550	0.72	430	1.24	725	1.17	575	1.34
610	0.80	460	1.25			600	1.39
700	0.84	475	1.26			625	1.41
		500	1.24			650	1.17
		600	1.28			675	1.18
		650	1.30				
$\langle\langle D\rangle/\langle H\rangle\rangle = 0.73(7)$		$\langle\langle D\rangle/\langle H\rangle\rangle = 1.23(5)$		$\langle\langle D\rangle/\langle H\rangle\rangle = 1.15(7)$		$\langle\langle D\rangle/\langle H\rangle\rangle = 1.26(9)$	

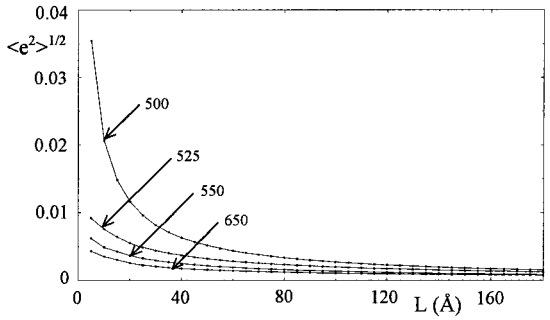

Figure 8. Root-mean-square microstrains ($\langle e^2\rangle^{1/2}$) versus L for ac-ZnO samples prepared at various temperatures.

that diameter and height growth rates are different. On the other hand for hn-ZnO, the values of n (6.8 for D and 9.6 for H) are much greater, and consequently the crystallite growth rate is much lower. Such a feature has already been observed during the initial stages of sintering of ZnO produced by oxidizing Zn vapor.[31] However, it must be noted that, contrary to the previous studies on the growth of grains during sintering, the present investigation is related to the study of the early stages of crystallite growth, i.e., on a nanometric scale. The values of n were considered constant over all temperature ranges. This was confirmed by additional experiments carried out at different temperatures.

Figure 9 shows the linear variation of ln D and ln H versus $1/T$ for hc- and ac-ZnO, from data given in Table 2, and for hn- and ox-ZnO, from data reported elsewhere.[12,13] The values of E_a/nR and E_a determined from the slopes are given in Table 1. Except for ox-ZnO, they are close to those calculated from the values of E_a/nR obtained at constant heating rate in the same temperature range [see section 3.2 (B)]. In addition, the activation energies obtained for hn-ZnO and ac-ZnO in the intermediate temperature range are much lower than those observed in the two other ranges. This result is related to the S-shaped behavior of their crystallite size growth (see Figure 5). On the other hand, the apparent activation energies for the mass transport are lower than those reported by Senda and Bradt[30] (224 kJ mol^{-1}). It can be concluded that for the four studies, the low energy for crystallite growth must be associated with a surface diffusion process and not grain boundary or lattice diffusion processes, which require more energy.[29]

(C) Specific Surface Area with Temperature. The values of the specific surface area, S_{BET}, of the grains for all annealed samples of hc- and ac-ZnO are given in Table 2. To describe the different features of the microstructural changes, it is worthwhile to compare S_{BET} to the specific surface areas, S_{XRD}, developed by the crystallites, with an average cylindrical shape. The latter can be calculated as follows from the values of $\langle D\rangle$ and $\langle H\rangle$ given in Table 2, assuming a monodisperse system:

$$S_{XRD} = [(4\langle H\rangle + 2\langle D\rangle) \times 10^4/(\langle D\rangle\langle H\rangle\rho)] \qquad (5)$$

where ρ is the density of ZnO (5.673 g cm^{-3}) and S_{XRD} is expressed in $m^2\ g^{-1}$. From Table 2, it is seen that, for the two samples, S_{BET} and S_{XRD} decrease with the annealing temperature, while S_{XRD} is always greater than S_{BET}.

(D) SEM Measurements. SEM micrographs of hc- and ac-ZnO samples obtained under isothermal conditions at two different temperatures are displayed in Figure 10. They show that grain growth is significant for the

(31) Moriyoshi, Y.; Komatsu, W. *J. Am. Ceram. Soc.* **1970**, 53, 671–675.

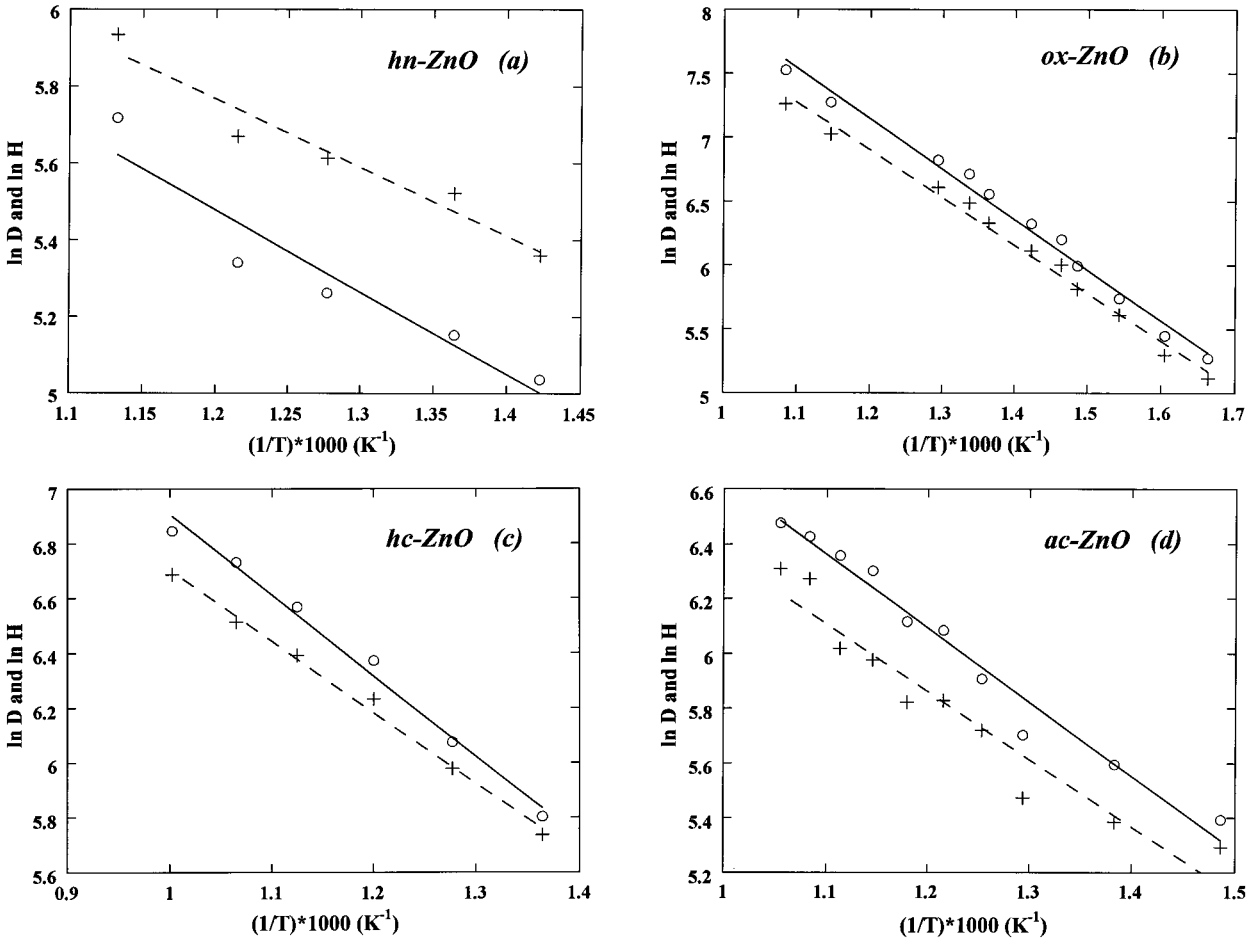

Figure 9. Plots ln D (○) and ln H (+) versus $1/T$ for samples prepared at various temperatures: (a) hn-ZnO, (b) ox-ZnO, (c) hc-ZnO, (d) ac-ZnO.

two ZnO samples in the small temperature range (~100 °C) of observations. In addition, the presence of strings of ZnO pearls (Figure 10a,c), as well as larger grains formed by cluster densification, are clearly observed. Such features have recently been described for the particle growths of $NaNbO_3$ and $ZrTiO_4$, whose mechanism is associated with surface diffusion followed by a "densification of the nanometric particle clusters and a neck size controlled particle growth".[32] The grain sizes deduced from SEM measurements (D_{SEM}) and BET measurements (D_{BET}) calculated from S_{BET} ($D_{BET} = 6 \times 10^4/\rho S_{BET}$) are reported in Table 2. It is obvious that D_{SEM} is lower than D_{BET}, which is due to the agglomeration process. Furthermore, D_{SEM} is greater than the crystallite size. This result demonstrates that several crystallites are aggregated into one grain. In addition, at high temperatures, the grains tend to have a mean hexagonal shape which is in agreement with the symmetry of ZnO.

4. General Concepts on Relationships between Oxide Crystallite/Particle Properties and Precursors

From the results obtained from both dynamic and isothermal modes, it is clear that the crystallite growth process depends on the temperature range and that from ~350 °C the aspect ratio $\langle D \rangle / \langle H \rangle$ is quasiconstant for the four ZnO samples, with the magnitude of the ratio depending on the precursor. Nevertheless, below this temperature, three of the samples (hn-, hc-, and ac-ZnO) exhibit a different thermal behavior characterized by an increase of the aspect ratio. This feature must be associated with the fact that the corresponding precursors decompose at low temperatures (<~250 °C). It can be thought that for these samples the crystallites are generated in an unstable state until, upon heating, they reach a stationary aspect ratio. Moreover, fundamental comments on relationships between the microstructural properties of ZnO and the nature of the precursor arise from this study performed on a nanometric scale.

(A) Crystallite Shape. For the four ZnO samples the crystallites are, on average, described by a cylindrical model, which is a good approximation for a hexagonal prism. This shape is in accordance with the crystal symmetry of ZnO, even though the precursor-crystal structure varies from a two-dimensional layered structure (hydroxide nitrate[33] and carbonate[34]) to a three-dimensional framework (oxalate[35] and acetate[36]).

(32) Leite, E. R.; Nobre, M. A. L.; Cerqueira, M.; Longo, E.; Varela, J. A. *J. Am. Ceram. Soc.* **1997**, 80, 2649−57.

(33) Louër, M.; Grandjean, D.; Weigel, D. *Acta Crystallogr.* **1973**, B29, 1703−1706.

(34) Wells, A. F. *Structural Inorganic Chemistry*, 5th ed.; Clarendon Press: Oxford, 1987; p 264.

(35) Kondrashev, Y. D.; Bogdanov, V. S.; Golubev, S. N.; Pron, G. F. *Zh. Strukt. Khim.* **1985**, 26, 90−93.

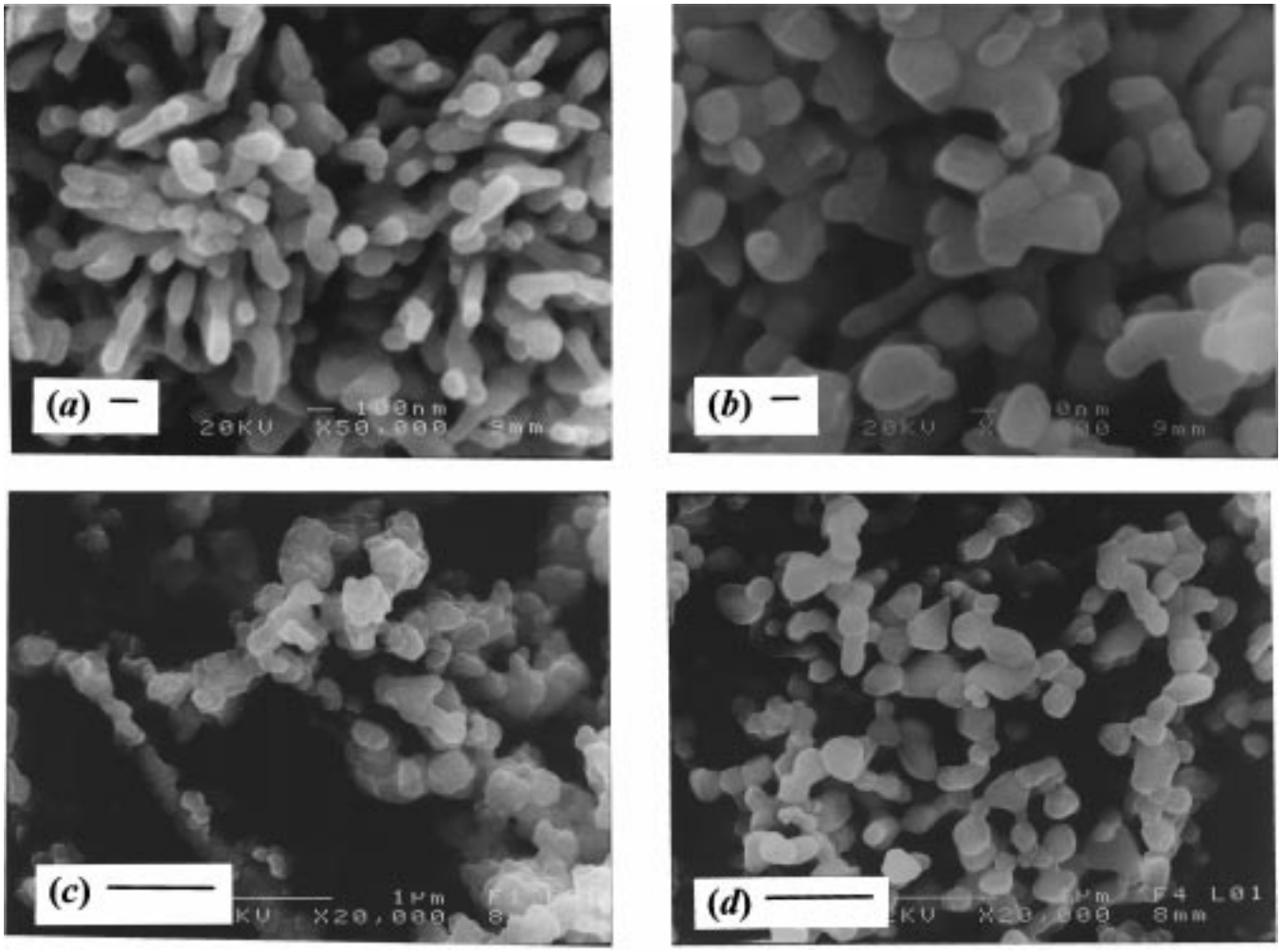

Figure 10. SEM micrographs of hc-ZnO obtained at (a) 616 °C and (b) 725 °C (bar = 100 nm) and ac-ZnO obtained at (c) 575 °C and (d) 675 °C (bar = 1 μm).

(B) Initial Crystallite Shape Anisotropy. As seen in Figure 6, different aspect ratios for the crystallites are observed immediately after the complete decomposition of the precursors. These aspect factors must originate from the mechanism of the decomposition reaction, which is itself influenced by the crystal structure of the precursor. These mechanisms are unfortunately not well-known, except perhaps for the "soft" topotactic decomposition of the layered compound $Zn_3(OH)_4(NO_3)_2$ into ZnO,[37] in which water and nitric acid molecules are gently formed from adjacent layers and then liberated between the layers.[38]

(C) Crystallite Shape Anisotropy in the Stationary Aspect Ratio Stage. As seen in Figure 6 and Table 3, even though $\langle D \rangle$ and $\langle H \rangle$ increase above 350 °C (see Figure 5), the aspect ratio $\langle D \rangle / \langle H \rangle$ is precursor dependent and it remains constant. This feature means that crystallite growth is homogeneous in all crystallographic directions; i.e., the nanodomains have a homothetic growth.

(D) Crystallite Growth Kinetics in the Stationary Aspect Ratio Stage. As seen in Table 1, the values of the kinetic exponent n and activation energy E_a are dependent on the precursor.

(E) Particle Agglomeration Process. Since nanodomains have been correctly characterized as a function of temperature, it is of interest to compare their characteristics to those derived from the BET method. As commented above, crystallites (or coherently diffracting domains) are characterized from X-ray diffraction line broadening, while the BET method gives information related to grains. Grains being constituted from crystallites, a comparison between the two (crystallite/grain) growth processes leads to information about particle agglomeration during the early stages of sintering. As suggested by Allred et al.,[39] the degree of agglomeration may be described through the ratio of the specific surface areas obtained from the BET method, S_{BET}, and the total surface area for a cylinder, S_{XRD} (see Table 2), as follows:

$$1/F = S_{BET}/S_{XRD} \qquad (6)$$

This ratio is a packing factor indicative of the relative crystallite surface area unavailable for nitrogen adsorption. It has been calculated as a function of temperature for the four ZnO samples prepared isothermally (Figure

(36) Ishioka, T.; Murata, A.; Kitagawa, Y.; Nakamura, K. T. *Acta Crystallogr.* **1997**, C53, 1029−1031.

(37) Auffrédic, J. P.; Ciosmak, D.; Louër, D.; Niepce, J. C. *Reactivity of Solids*; Dyrek, K., Haber, J., Nowotny, J., Eds; Elsevier: Amsterdam, 1982; Vol. 2, pp 826−830.

(38) Auffrédic, J.-P.; Louër, D. *Thermochim. Acta* **1978**, *22*, 193−196.

(39) Allred, V. D.; Buxton, S. R.; McBride, J. P. *J. Phys. Chem.* **1957**, 61, 117−120.

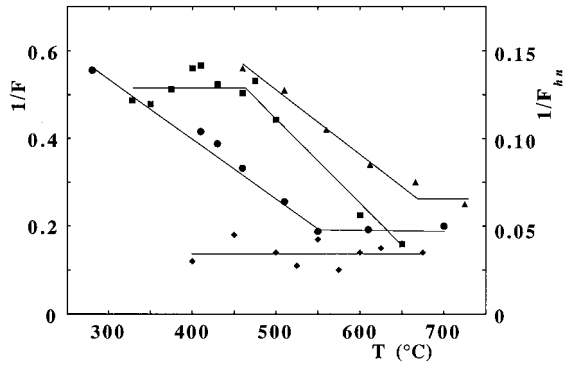

Figure 11. Packing factors 1/*F* as a function of temperature: (■) ox-ZnO, (▲) hc-ZnO, (◆) ac-ZnO, (●) hn-ZnO ($1/F_{hn}$).

11). The thermal behavior of this factor is different for the four samples. An interesting feature is that there is a sudden change in the slope of the initial linear region for three of the samples. Among them, the same behavior (1/*F* decreases first and then is constant) is observed for hn-ZnO and hc-ZnO, whose precursors have a layer-type structure. For ox-ZnO, 1/*F* is constant first and then decreases, while for ac-ZnO the packing factor remains constant over the temperature range considered. It should be noted that for the two last samples the structure of the precursors is three-dimensional.

From the definition of the packing factor (eq 6) it is seen that the thermal behavior of 1/*F* is related to a competition between the growth of crystallites and grains. A decrease would mean that the crystallites grow faster than the grains, while a constant value would correspond to similar growth rates. The fact that 1/*F* for ac-ZnO (Figure 11) remains constant in the temperature range investigated may well be fortuitous, because outside this range no relevant size measurements could be obtained due to the limits of line-broadening analysis.

Finally, all these observations can be summarized as follows:

(1) The crystallite shape is related to the symmetry of ZnO. It is not precursor dependent.

(2) The initial crystallite shape anisotropy is precursor-dependent.

(3) In the stationary aspect ratio stage (>∼350 °C), the crystallites grow with a similar shape. The magnitude of the aspect ratio depends on the precursor.

(4) The kinetic process of the crystallite growth is precursor-dependent.

(5) The particle agglomeration process during the early stage of crystallite growth is precursor-dependent.

5. Concluding Remarks

From the application of modern powder diffraction techniques the microstructural properties, on a nanometric scale, of four powders of zinc oxide prepared from the thermal decomposition of different inorganic precursors have been confidently determined, in both dynamic and isothermal experimental conditions. Two domains of crystallite growth, an initial stage observed in situ for three samples and a next stage, over most of the remaining temperature range investigated, observed in both in situ and ex situ experiments arose from these studies. In the second stage the aspect ratio *D*/*H* is remarkably stationary, which corresponds to a homothetic growth of the crystallites. It has been shown that, except for the crystallite shape related to the hexagonal symmetry of ZnO, the other microstructural properties of ZnO depend on the nature of the precursor. Thus, a memory effect must be invoked to explain these observations. Clearly, a complete explanation should necessitate a detailed knowledge of both the crystal structure of the precursors and the mechanisms of the decomposition reaction giving rise to the oxide. However, some elements driving the processes can be discussed from the case of hn-ZnO, which results from a topotactic reaction. In this kind of reaction, crystallites obtained from the decomposition of the precursor are constrained inside a pseudomorph, which is a reminiscent of the precursor crystal shape. Oxide crystallites are first constrained to grow from a coalescence process inside the pseudomorph limits, until the memory of the initial precursor crystal-shape can exist. Beyond this limit, the constraints do not hold and the growth of the crystallites is then essentially governed by the free competition between the growth of the two types of particles (crystallite and grain). It is likely that this phenomenon, related to some "genetic" transmission, contributes to the sudden changes of particle agglomeration behavior observed when the temperature increases. hc-ZnO formed from a precursor with a layer structure should have similar features. For the two other samples there is not enough experimental evidence to explain the corresponding particle agglomeration behavior, which is however initially governed by similar crystallite and grain growth rates and, then, by a faster crystallite growth with respect to grain growth, at least for ox-ZnO.

To conclude, to our knowledge, this is the first time that such a detailed study, on a nanometric scale, of the early stages of crystallite growth has been carried out for a series of oxide samples obtained from different precursors. The careful use of modern diffraction pattern fitting methods combined with an interpretation of line broadening has allowed us to investigate the microstructural properties of four ZnO samples as a function of temperature and, subsequently, to state some general concepts on their dependence on the nature of the precursor. Finally, the study illustrates the power of TDXD used for a quantitative evaluation of crystallite sizes in a dynamic process.

Acknowledgment. The authors are indebted to C. Magnenet for her help in the isothermal studies and G. Marsolier for his technical assistance in diffraction data collection. One of the authors (N.A.) is indebted to the Conseil Régional de Bretagne (France) and to the International Centre for Diffraction Data (Newtown Square, PA) for financial support.

CM980132F